1974

Natural convection flow visualization and heat transfer from a horizontal circular disk.

O'Connor, Joseph Michael.

Monterey, California. Naval Postgraduate School

NATURAL CONVECTION FLOW VISUALIZATION AND HEAT TRANSFER FROM A HORIZONTAL CIRCULAR DISK

Joseph Michael O'Connor

NAVAL POSTGRADUATE SCHOOL
Monterey, California

THESIS

NATURAL CONVECTION FLOW VISUALIZATION
AND HEAT TRANSFER FROM A HORIZONTAL
CIRCULAR DISK

by

Joseph Michael O'Connor

June 1974

Thesis Advisor: M. D. Kelleher

SECURITY CLASSIFICATION OF THIS PAGE (When Data Entered)

REPORT DOCUMENTATION PAGE

READ INSTRUCTIONS BEFORE COMPLETING FORM

1. REPORT NUMBER	2. GOVT ACCESSION NO. / 3. RECIPIENT'S CATALOG NUMBER
4. TITLE (and Subtitle): Natural Convection Flow Visualization And Heat Transfer From A Horizontal Circular Disk	5. TYPE OF REPORT & PERIOD COVERED: Master's Thesis; June 1974
	6. PERFORMING ORG. REPORT NUMBER
7. AUTHOR(s): Joseph Michael O'Connor	8. CONTRACT OR GRANT NUMBER(s)
9. PERFORMING ORGANIZATION NAME AND ADDRESS: Naval Postgraduate School, Monterey, California 93940	10. PROGRAM ELEMENT, PROJECT, TASK AREA & WORK UNIT NUMBERS
11. CONTROLLING OFFICE NAME AND ADDRESS: Naval Postgraduate School, Monterey, California 93940	12. REPORT DATE: June 1974
	13. NUMBER OF PAGES: 60
14. MONITORING AGENCY NAME & ADDRESS (if different from Controlling Office): Naval Postgraduate School, Monterey, California 93940	15. SECURITY CLASS. (of this report): Unclassified
	15a. DECLASSIFICATION/DOWNGRADING SCHEDULE

16. DISTRIBUTION STATEMENT (of this Report)

Approved for public release; distribution unlimited.

17. DISTRIBUTION STATEMENT (of the abstract entered in Block 20, if different from Report)

18. SUPPLEMENTARY NOTES

19. KEY WORDS (Continue on reverse side if necessary and identify by block number)

Natural Convection
Flow Visualization
Acid-Base pH Indicator
Horizontal Disk
Cylindrical Enclosure

20. ABSTRACT (Continue on reverse side if necessary and identify by block number)

This study of natural convection incorporates a flow visualization procedure, with heat transfer experiments on a circular mirror like surface, in a cylindrical enclosure.

A flow visualization procedure using Thymol Blue sodium salt in distilled water was conducted. Photographs are presented which show the cellular flow pattern on the horizontal test surface and the nature of the flow in the plume. Problems applying the flow visualization technique are

DD FORM 1 JAN 73 1473 EDITION OF 1 NOV 65 IS OBSOLETE
S/N 0102-014-6601
(Page 1)

SECURITY CLASSIFICATION OF THIS PAGE (When Data Entered)

20. (cont'd)

discussed. Photographs are presented which show the effect of voltage on a laminar natural convection flow in the plume.

From the flow visualization, it was observed that transition to turbulence in the plume occurs in the range of Grashof numbers (based on test surface diameter) from 8.5×10^6 to 1.3×10^7.

Experimental results are presented for the heat transfer from the horizontal circular disk. This data was compared to previously reported results and the agreement was good.

Natural Convection Flow Visualization And Heat Transfer From A Horizontal Circular Disk

by

Joseph Michael O'Connor
Lieutenant, United States Navy
B.S., College of Charleston, 1966

Submitted in partial fulfillment of the
requirements for the degree of

MASTER OF SCIENCE IN MECHANICAL ENGINEERING

from the

NAVAL POSTGRADUATE SCHOOL
June 1974

ABSTRACT

This study of natural convection incorporates a flow visualization procedure, with heat transfer experiments on a circular mirror like surface, in a cylindrical enclosure.

A flow visualization procedure using Thymol Blue sodium salt in distilled water was conducted. Photographs are presented which show the cellular flow pattern on the horizontal test surface and the nature of the flow in the plume. Problems applying the flow visualization technique are discussed. Photographs are presented which show the effect of voltage on a laminar natural convection flow in the plume.

From the flow visualization, it was observed that transition to turbulence in the plume occurs in the range of Grashof numbers (based on test surface diameter) from 8.5×10^6 to 1.3×10^7.

Experimental results are presented for the heat transfer from the horizontal circular disk. This data was compared to previously reported results and the agreement was good.

TABLE OF CONTENTS

LIST OF TABLES

LIST OF FIGURES

NOMENCLATURE

Symbol	Description	Units
D	Heated surface diameter	Inches or ft
g	Acceleration of gravity	Ft/sec^2
h	Convection heat transfer coefficient	$BTU/Hr/Ft^2/^oF$
H	Height of cylindrical tank	Inches or ft
K	Thermal conductivity of 304 stainless steel	$BTU/Hr/Ft/^oF$
K_f	Thermal conductivity of test fluid - distilled water	$BTU/Hr/Ft/^oF$
R	Radius of cylindrical tank	Inches or ft
T_b	Bulk temperature of fluid	^oF
T_s	Test section surface temperature	^oF
δT	Temperature difference between test surface and fluid $(T_s - T_b)$	^oF
T_8	Temperature measured in stainless steel test section at a location 0.227 inch from test surface	^oF
T_{11}	Temperature measured in stainless steel test section 1.727 inch from test surface	^oF
δT_c	Temperature difference in test section $(T_{11} - T_8)$	^oF
T_f	Film temperature $\frac{T_s + T_b}{2}$	^oF
δX	Distance in stainless steel test section between thermocouple no. 8 and thermocouple no. 11	Inches or ft
$W_{subscript}$	Uncertainty in variable denoted by subscript, for example $W_{\delta T}$ is uncertainty in δT.	Units of variable denoted by subscript.

α	Fluid thermal diffusivity	Ft^2/sec
β	Fluid coefficient of thermal expansion	$1/^oF$
ν	Fluid kinematic viscosity	Ft^2/sec

Dimensionless Numbers

Gr	Grashof number based on test surface diameter	$\frac{g\beta D^3 \delta T}{\nu^2}$
Gr_H	Grashof number based on cylindrical tank height	$\frac{g\beta H^3 \delta T}{\nu^2}$
Gr_R	Grashof number based on cylindrical tank radius	$\frac{g\beta R^3 \delta T}{\nu^2}$
Nu	Nusselt number based on test section diameter	hD/K_f
Pr	Fluid Prandtl number	ν/α
Ra	Rayleigh number	GrPr

ACKNOWLEDGMENT

The author wishes to thank Professor M.D. Kelleher, his thesis advisor, for his guidance and advice in this endeavor.

He wishes to express his appreciation to Mr. Dennis Daigle of the Educational Media Department photography lab. It was through his efforts that the photography of the flow visualization in this study was accomplished.

The author would also like to thank Mr. George Bixler, Mr. Jack McKay, and Mr. Roy Edwards, all of the Mechanical Engineering Department for their advice on design and their timely work on the experimental apparatus.

A special word of thanks and sincere appreciation to my wife, Debby, without whose understanding and patience and assistance in preparing and typing of the rough copy of this work, the entire undertaking would have been extremely difficult.

I. INTRODUCTION

A. BACKGROUND

If an experimenter spends any time reviewing the recent literature on natural convection in enclosures, he will become aware of the many variations of geometry and heat input situations that this field of study encompasses. In approaching the study of natural convection in enclosures, a logical first step must be to decide upon a geometrical configuration. The next question to be answered will be, "should heat transfer aspects be studied or should an attempt be made at characterizing the flow?". In beginning this thesis study, a circular test section in a cylindrical container with an aspect ratio of 1.0 was selected. This configuration easily lends itself to both heat transfer and flow visualization studies. Heat transfer data could be compared with existing results. A flow visualization technique using an acid - base pH indicator had been used previously with a similar geometrical configuration. It was intended that the data obtained from this work would serve as a basis for future experiments that would show the effects of surface cavities on heat transfer. Also the problems encountered and the procedures involved in implementing the flow visualization technique would be documented to serve as a guide to future experimenters.

Prior to describing the experiment itself several papers that represent the broad spectrum of natural convection heat transfer in enclosures should be considered. Ostrach [1] presents a very extensive discussion of natural convection in enclosures and a comprehensive review of the experimental and theoretical work through 1969.

In 1969, Catton and Edwards [2] presented an analytical method to predict heat transfer rates in fluids contained in vertical cylinders heated on a horizontal bottom and cooled on a horizontal top. A relation for Nusselt number in terms of Rayleigh number was presented. A "wave number" was defined which depends on the height to diameter ratio and the Rayleigh number is determined by this wave number. Very high and very low height to diameter ratios were discussed. They later investigated the initiation of convection in finite right circular cylinders [3]. Convection in cylindrical layers heated from below was discussed by Charlson, et al [4]. In early 1972, Plows [5] presented a discussion of the hexagonal cell patterns observed by Benard in a horizontal fluid layer heated from below. He developed numerical results based on a two dimensional model that satisfies the Boussinesq approximation. Calculations were made for three configurations: (1) a horizontal unbounded region, (2) a region bounded by two parallel vertical walls and (3) a cylindrical region. Stork and Muller [6] conducted experiments on a fluid heated from below and presented a flow visualization using aluminum particles.

Szekely and Todd [7] discussed natural convection in a rectangular cavity and compared their experimental data with previously reported results. Ostrach [1] discussed the results which Szekely and Todd used for a basis of comparison.

The natural convection plume arising from a horizontal line source of heat has been the subject of several papers by Gebhart and Pera. In 1970, Gebhart, et al [8] developed a theoretical analysis of this problem, including a discussion of the boundary conditions. The results of experiments with plumes were discussed. Pera and Gebhart [9] investigated the stability of plumes, discussed the numerical solution to the problem and described associated experiments. Fujii, et al [10], presented a review

of the experimental results for plumes in air, water and spindle oil. Photographs showing plume motion in spindle oil were presented. The theoretical problem was treated and the work of Gebhart, et al [8] discussed.

An interesting paper by Lloyd, et al [11] described the background for work dealing with natural convection mass transfer adjacent to vertical plates. The experimental apparatus and measurement technique were discussed. The agreement between theory and experimental results was excellent.

In 1968, Hussar and Sparrow [12] published a short paper on the patterns of free convection flow adjacent to horizontal surfaces. They employed a flow visualization technique introduced by Baker [13]. The purpose of their paper was to present flow visualization of various free convection flow fields in order to provide some insight into the effect of geometry on the flow. Their results included flow patterns for square, rectangular, triangular and circular planforms. The flow patterns presented were in the range of Rayleigh numbers from 10^6 to 10^8. Natural convection flow patterns on a horizontal circular plate were presented by Hahne [14] in 1969. His work was in the Rayleigh number range from 10^9 to 10^{13}. The experiments were carried out with carbon dioxide in the supercritical region. Wragg and Looma [15] pursued experiments using a circular geometry developing correlations for heat and mass transfer at horizontal surfaces. Goldstein, et al [16] also carried out experiments for natural convection adjacent to horizontal surfaces. Their results for both heat and mass transfer were presented graphically and compared with the results of Wragg and Looma and with heat transfer correlations of Fishenden and Saunders [17] and Mikheyev [18]. The point is made that the basis of Mikheyev's correlation is not described in the literature and little is known about the experiments that served as a basis for the

Fishenden and Saunders correlation. Natural convection from isothermal flat plates in air was dealt with by Hussan and Mohamed [19]. Their experiments were conducted for plates with inclinations varying from the horizontal "facing upwards" position through the vertical position to the horizontal "facing downwards" position. For hot plates facing upwards the following equation represented their experimental data to within 15%:

$$Nu = 0.12\ (GrPr)^{1/3} \qquad (1)$$

Sparrow, et al [20] using Baker's electrochemical flow visualization technique directly observed thermals rising from heated horizontal surfaces and presented a detailed discussion of the periodicity and frequency of thermal generation. The experimental results agreed with an analytical model developed by L. N. Howard which is discussed in Sparrow's paper.

Torrance, et al [21] presented an experimental model designed to study laminar flows induced by a simulated fire. This experiment used air in a cylindrical enclosure with a heated disk in the center. In a companion paper, Torrance et al [22], the experimental results were compared with values determined from a numerical study. A plot of the Nusselt number based on a disk diameter versus the Grashof number shows excellent agreement between experimental and theoretical results. It should be noted that in the experimental work, turbulence was observed for Grashof numbers, based on enclosure height, greater than 1.2×10^9. These papers and many others that deal with fire research are discussed by Lee and Hellman [23].

Recording the heat transfer from a horizontal circular disk, with a mirror finish in a cylindrical enclosure, Duncan [24] obtained the following correlation:

$$Nu = 0.31\ (Ra)^{0.30} \qquad (2)$$

He presented his results in comparison with the experimental and theoretical results obtained by Torrance, et al [22].

The previous discussion was designed to provide the reader with a general overview of the studies of natural convection in enclosures. The cited references to papers are not to be construed as being all inclusive, but as representative of what has been done in the area of natural convection in enclosures.

B. THESIS OBJECTIVES

The objectives of this study were:

1. To implement the flow visualization work of Hussar and Sparrow [12] for circular configurations. Baker's [13] technique for visualization would be used to obtain flow patterns for various Grashcf numbers.
2. To obtain natural convection heat transfer data from a mirror-like surface of circular geometry. This data would be compared to the results of Torrance, et al [22], and to the correlations of other investigators.

It is intended that this work serve as a basis for future flow visualization and heat transfer studies that will show the effect of surface condition on heat transfer by natural convection.

II. EXPERIMENTAL APPARATUS

A. DESIGN CONSIDERATIONS

A stainless steel cylinder installed in the center of a cylindrical tank, flush with the tank floor, served as a test surface. A copper block, housing a resistance heater which provided a controllable heat source, was attached to this cylinder. Using a calibrated resistor in series with the heater and a power supply, the input to the heater could be accurately determined. Temperatures were recorded at four locations in the stainless steel cylinder and the bulk temperature of the fluid in the tank was measured.

Figure 1 is a cross sectional view of the tank, test section and heater assembly, and Figure 2 is an overall view of the complete apparatus including instrumentation. Figure 3 shows the assembled apparatus. The tank, test section and heater arrangement were constructed utilizing material available in the Mechanical Engineering Department shops and components from the apparatus used by MacKenzie [25].

Several criteria were established to serve as basic guidelines for the apparatus design:

(1) The enclosure height was to be equal to the enclosure radius. This aspect ratio was convenient to work with and would give results which could be directly compared to the experimental and theoretical results presented by Torrance, et al [22] and Duncan [24].

(2) The test surface radius was to be equal to one-tenth the enclosure height. This ratio was also a geometrical restriction which was motivated by the work of Torrance, et al [21].

(3) Heat loss due to conduction had to be minimized as much as possible.

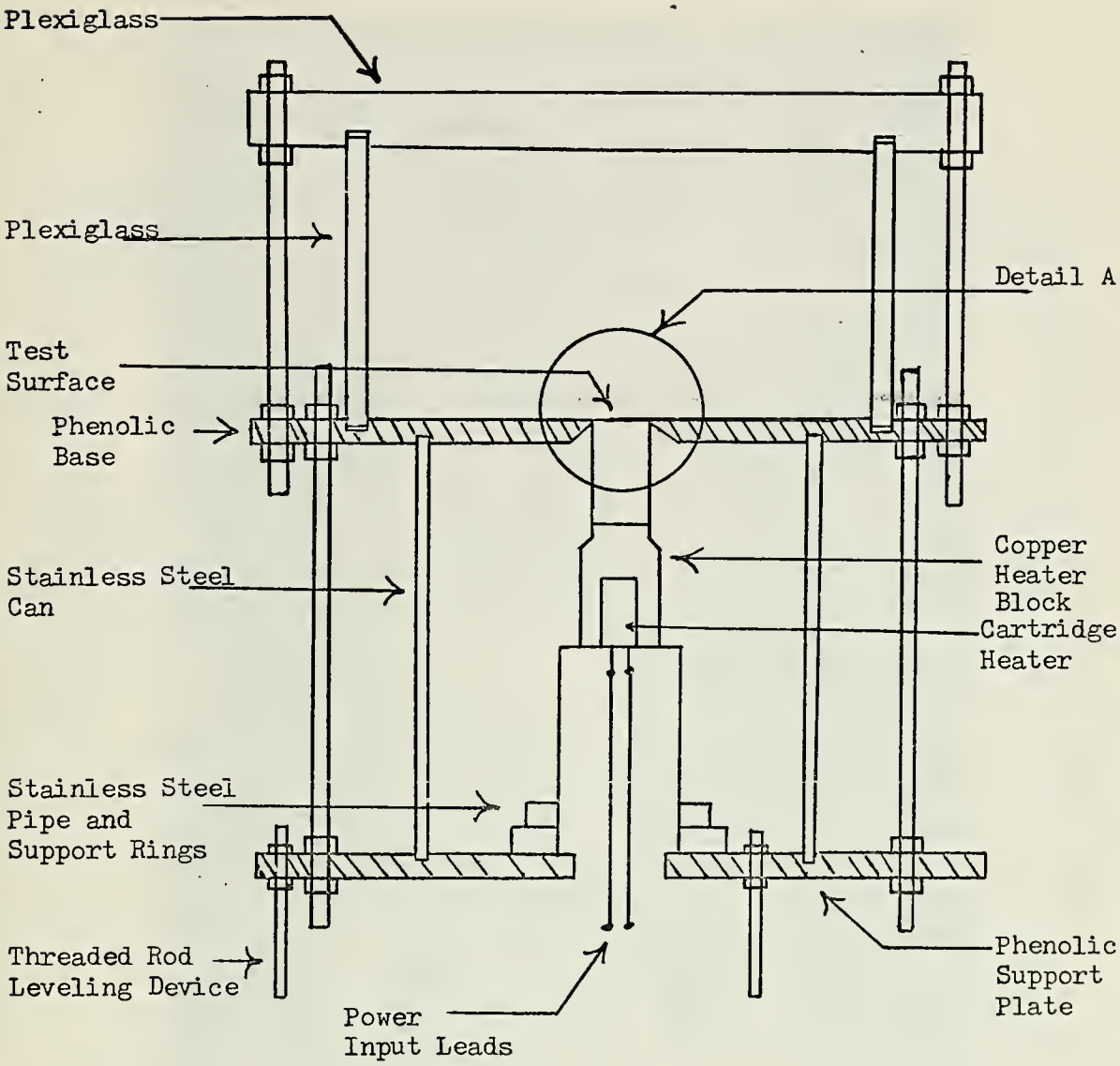

DETAIL A

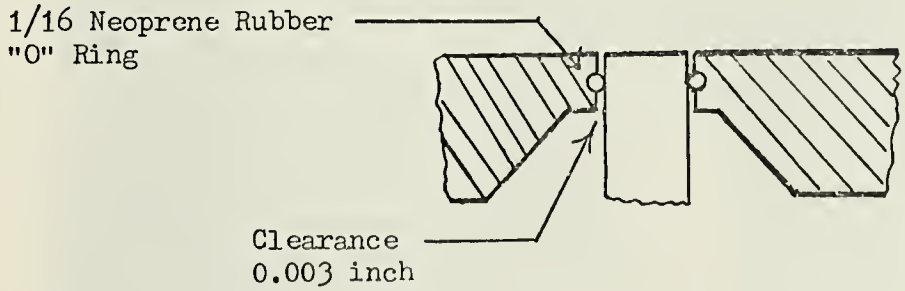

Figure 1. Cross Sectional View of Tank, Test Section and Heater Assembly

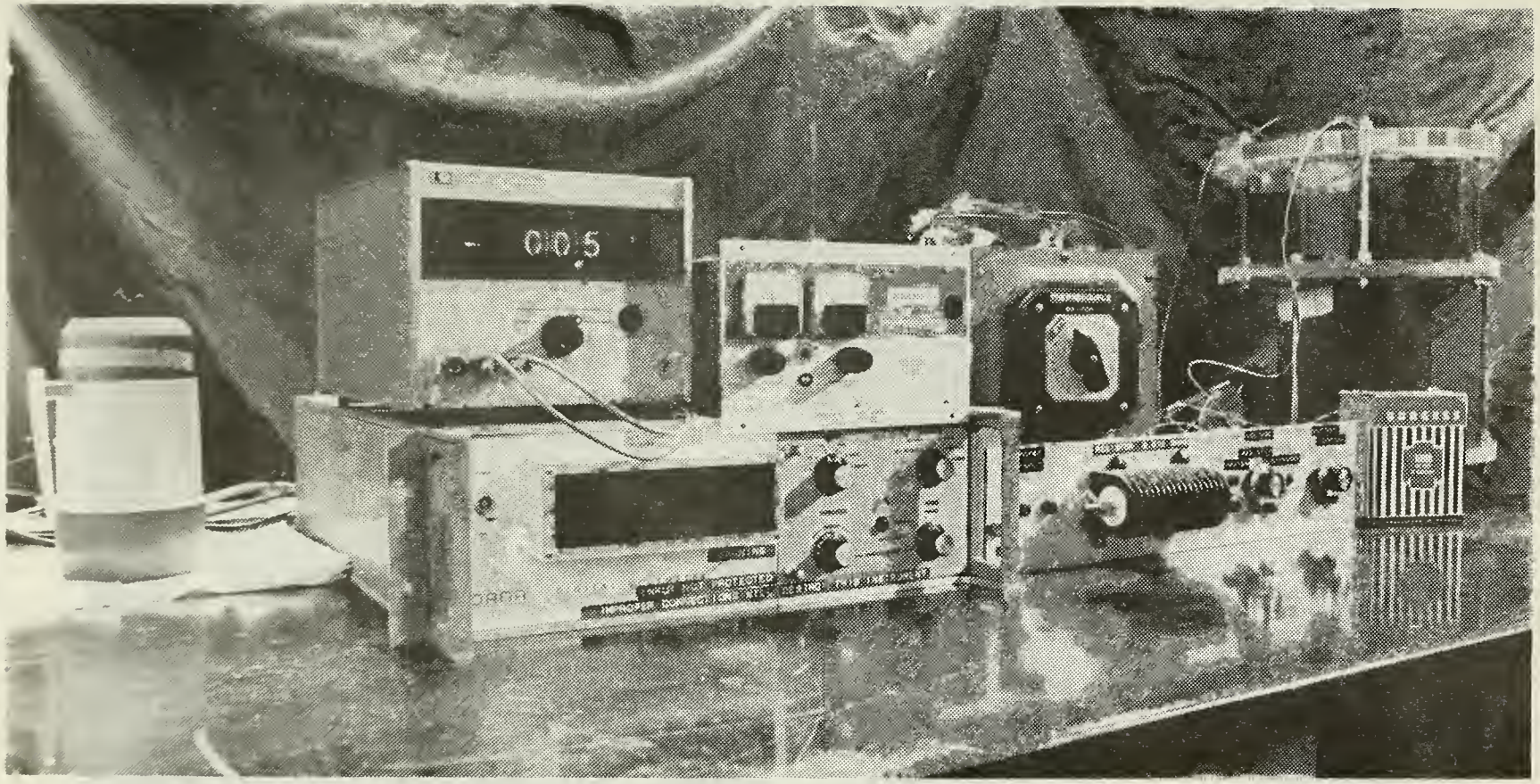

Figure 2. Photograph of Complete Apparatus Including Instrumentation

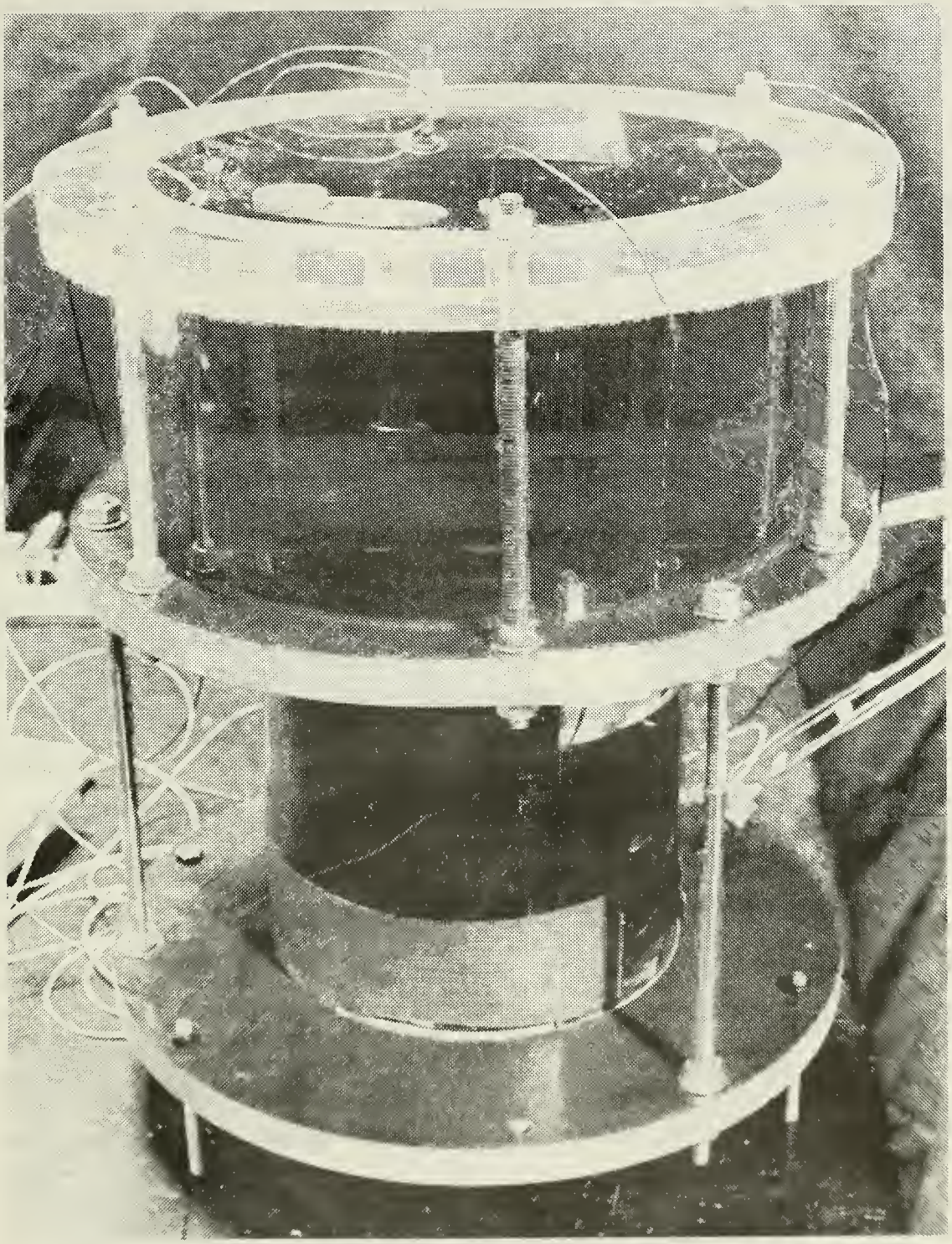

Figure 3. Photograph of Assembled Experimental Unit

(4) The flow visualization technique, utilizing a pH acid-base indicator, introduced by Baker [13] would be used.

During the initial phase of apparatus design, test section designs used by Duncan [24] and MacKenzie [25] were examined. Both made use of a solid cylinder to attempt to achieve one dimensional heat flow. Duncan used a stainless steel cylinder with a flanged top forming the test surface. In discussing his results, Duncan indicated the problems that developed due to this design and how the heat transfer results were affected. MacKenzie [25] used a similar cylinder-heater assembly.

It was decided that the use of a cylinder to achieve one dimensional heat flow was feasible if radial conduction losses could be minimized. The cylinder would be silver soldered to the heater section. This test section-heater assembly would be rigidly supported at the base of the heater. Because the heat flow through the cylinder would be the basis for the calculation of the convection heat transfer coefficient, the thermal conductivity of the material used had to be accurately known. For this reason, and because of its machinability, 304 stainless steel was chosen.

Baker [13] used an acid-base pH indicator, thymol blue, in distilled water to accomplish flow visualization. This electrochemical technique utilizes a small voltage across electrodes to produce a change in the ionic concentration of a solution. The indicator which is red-orange in an acid solution, changes to a blue color in the vicinity of the negative electrode, when voltage is applied across the solution. It is claimed that this color change does not disturb the flow, but becomes part of the flow, enabling an observer to clearly "see" the flow pattern.

Preliminary tests using this flow visualization technique indicated that the 304 stainless steel test section would perform satisfactorily

when used as the negative electrode. Also stainless steel shim stock was ideal for use as a positive electrode since it did not discolor, oxidize or corrode when left in the thymol blue solution for long periods of time.

A material with a very low thermal conductivity was needed for the bottom of the tank since this material would be in contact with the test section. Phenolic was readily available and it was used by MacKenzie [25] in a similar apparatus. Thus it was known to be strong enough to tolerate the tensile forces that might be applied in achieving a watertight tank arrangement. The stainless steel cylinder was centered in the bottom of the tank and the phenolic was machined to a tight fit and bevelec to minimize conduction area. In order to insure a watertight seal a 0.0625 inch Neoprene rubber "O" ring lubricated with silicone vacuum grease was installed in the phenolic bottom plate.

The optical properties of plexiglass made it the logical choice for the tank top and sides.

B. TEST SECTION AND HEATER ASSEMBLY

The 2-inch stainless steel cylinder as shown in Figure 4 was machined from a 1-inch diameter 304 stainless steel rod to a 0.8960 inch diameter. Four 0.041 inch diameter holes were drilled a depth of 0.375 inch, separated axially 0.5 inch and 90° apart for thermocouple installation. The stainless steel cylinder was silver soldered to a copper block which served as a housing for the heater. A 250 watt, 120 volt Watlow Firerod Cartridge heater was installed in the copper block. A 3.375 inch section of 2.0 inch diameter stainless steel pipe, with a 2.0 inch outside diameter and 0.625 inch inside diameter ring welded to one end was attached to the copper block and heater by two 0.75 inch machine screws. This

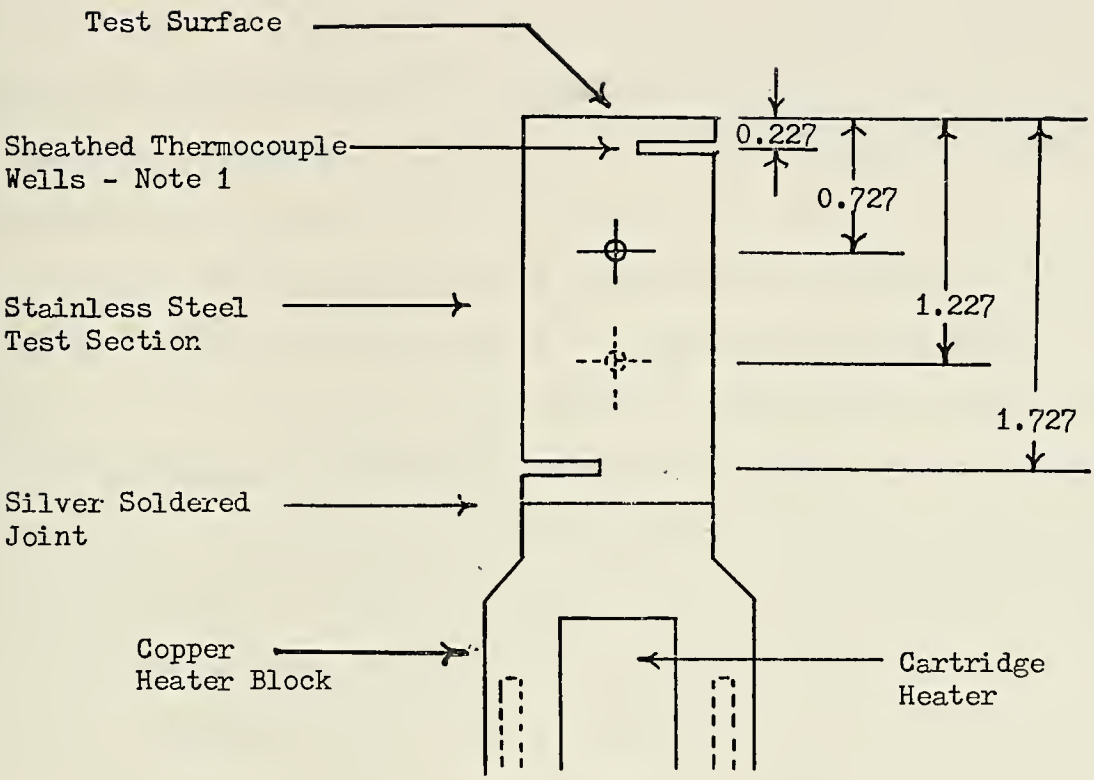

Notes:

1. Diameter of sheathed thermocouples 0.041 inch.

Figure 4. Test Section - Heater Assembly

arrangement provided a rigid support for the test section-heater assembly. Also it eliminated the necessity for any other metal to metal contact with the test section.

Several layers of asbestos paper were placed between the heater base and stainless steel ring. The other end of the stainless steel pipe was fitted into two stainless steel rings machined to a tight fit to the pipe. These rings were securely bolted to a 12.0 inch diameter phenolic plate that served as a support plate for the entire system. The test section and heater arrangement was enclosed in a 6.25 inch diameter stainless steel can, 0.125 inch thick.

Since every step of the design was concerned with heat loss, an effective insulation method for the test section-heater assembly had to be devised. A 6.5 inch preformed section of asbestos pipe lagging block, 1.0 inch thick, 2.0 inch inside diameter, was fitted around the stainless steel pipe and secured with insulating tape. The heater assembly and a portion of the test section enclosed in the asbestos block were wrapped with asbestos paper and packed with fiberglass insulation. Several layers of Flex-Min K insulation were fitted around the remaining portion of the test section and the entire assembly was wrapped with Flex-Min K insulation in layers, completely insulating the interior of the stainless steel can. Fiberglass and powdered magnesium oxide were packed into the interior of the pipe around the heater leads. Several layers of asbestos paper covered the opening in the bottom and were placed between the phenolic base plate and the stainless steel ring holding the pipe section.

C. INSTRUMENTATION

1. Temperature Measurement

The temperature distribution in the stainless steel test section was determined using four ungrounded junction, Copper Constantan thermocouples, sheathed in stainless steel.

The bulk fluid temperature was determined using five Copper Constantan thermocouples manufactured using a Dynatech welder. These thermocouples were wired in parallel into an insulated switching box. The arrangement automatically gave an average output. The sheathed thermocouples were difficult to manipulate and subject to twisting, and thus shorting, giving erroneous readings. To avoid problems the sheathed thermocouple leads were securely fastened to a Jones bar arrangement and the more flexible wire used for the bulk temperature thermocouples was used as extension wire into the switching box. A single thermocouple reference junction was used in a distilled water ice bath. This reference was also wired to the switching box. The output from the thermocouples was read on a Dana digital voltmeter accurate to 0.001 millivolt.

2. Power to Heater

A Lambda regulated power supply was used to provide input voltage to the heater. A calibrated resistor was placed in series with the power supply and heater. With this arrangement, a voltage reading across the resistor and across the heater were taken. Knowing the voltage, and resistance, the current through the circuit could be determined. The product of this current and the voltage across the heater gave the input power. This value could be accurately reset for different runs. The voltage across the heater and across the calibrated resistor were determined using a Hewlett-Packard 3430A digital voltmeter, with an accuracy of 0.01 volts.

3. Voltage Across Electrodes

The flow visualization technique required from 4 to 8 volts depending upon the input power to the heater. A 45 volt DC battery was used for voltage source. It was wired to a 50K ohm rheostat. The positive side was connected to the one inch by six inch section of stainless steel shim stock at the top of the tank. The stainless steel test section served as the negative electrode.

III. EXPERIMENTAL PROCEDURE

A. TEST SURFACE PREPARATION

It was very important that the test surface be free from any machine marks and scratches that could influence the flow pattern. It was decided to mirror polish the surface. The machine marks were removed using a Buehler Metallurgical Manual grinder. Both 0 emery polishing paper and 3/0 emery polishing paper were used. The final mirrorlike finish was accomplished using a one micron diamond compound wheel.

Once the desired finish was obtained, measurements were taken to determine the location of the center of the holes for the thermocouples in relation to this surface. An engineering flat and a scale readable to 0.0005 inch were used for these measurements as shown in Figure 4.

B. APPARATUS ASSEMBLY

The apparatus consisted of two main components: the test section-heater assembly and the tank. The test section-heater assembly, as described previously, was securely bolted to the phenolic base plate and once the insulation was in place and the can installed, the phenolic plate that served as the bottom of the tank was carefully fitted to the test section. This plate was secured to the base plate by three threaded rods 120° apart. The rods also served as a means of adjusting the phenolic bottom plate, so that the test surface was level with the bottom plate.

The cylindrical plexiglass container was then put in place and the top installed. Rubber gaskets were used at the top and bottom of the cylindrical enclosure to insure that the tank was watertight. Six

threaded rods, 60° apart were used to secure the top plate to the bottom plate of the tank.

Thus it was possible to remove the top plate and cylindrical enclosure without disturbing the test section.

The bulk temperature thermocouples were inserted into the tank through small holes in the tank top.

It should be noted that the test section was cleaned with acetone prior to filling the unit. All surfaces exposed to the fluid were washed with a standard laboratory cleaning solution and thoroughly rinsed with distilled water.

C. FLUID PREPARATION

The test fluid was distilled water with less than one gram of thymol blue sodium salt pH indicator dissolved in it. The fluid was prepared as described by Baker [13], but the thymol blue sodium salt was used because of its solubility in water. Initial samples prepared using thymol blue powder did not dissolve completely. Even when dissolved using a mortar and pestel and heated, the solubility was not greatly improved. It was because the fluid had to be filtered to remove undissolved particles that the thymol blue sodium salt was used. It was found that solutions made by dissolving 0.2g of thymol blue sodium salt in one liter of distilled water yielded good color changes. This quantity amounts to approximately 0.02 per cent by weight of the solution. The solutions were titrated to the endpoint using 0.1 normal NaOH and one drop of 0.1 normal HCl was added to bring the solution back to the acid side of the pH indicator.

The fluid could be poured into the tank through a one inch diameter hole provided for that purpose. Fluid removal was accomplished using a siphon.

D. TEST PROCEDURE

1. Temperature

The input power setting to the heater was the independent variable for the system. Five representative settings were determined and all calculations and photographs were taken at these settings.

A complete data run consisted of starting at the lowest input setting, waiting until steady state was reached, repeating the procedure for each increasing setting. Once the highest setting had reached steady state, the power input was decreased to the next lower setting, waiting for steady state, repeating until the starting setting was reached. Thus a check for hystersis was part of each run.

The data recorded for each setting was the bulk temperature and the temperature of the individual thermocouples in the test section. The flow was observed during this time, but the temperature readings were taken only when the voltage across the electrodes was off.

Initially, temperature readings were recorded every hour, except during the night. Steady state was determined when the temperature change in the bulk temperature and the temperature of the thermocouple nearest the heater changed less than $0.5^{\circ}F$ per hour.

Torrance, et al [21] in the design of their experimental apparatus used a wall temperature which was an average of the temperature of the container walls and floor for calculations of the Nusselt and Grashof numbers. In order to determine the effect of wall temperature, the bulk temperature thermocouples were taped to the apparatus walls for one run.

2. Determination of the Nusselt and Grashof Numbers

For each run, at all input settings, the temperature distribution in the stainless steel test section was plotted and found to be linear. The surface temperature could be determined within $0.5^{\circ}F$ from the plot

of temperature versus thermocouple location by extrapolation, as shown in Appendix B. A simple energy balance at the surface using Fourier's Law of Conduction yields:

$$K \frac{\delta T_c}{\delta X} = h (T_s - T_b) \tag{3}$$

The Nusselt number was obtained from the definition:

$$Nu = \frac{hD}{K_f} \tag{4}$$

The Grashof number was calculated using the diameter of the heated test surface as the characteristic length.

$$Gr = \frac{g \beta D^3 (T_s - T_b)}{\nu^2} \tag{5}$$

All fluid properties were evaluated at the film temperature as defined:

$$T_f = \frac{T_s + T_b}{2} \tag{6}$$

The properties of the stainless steel test section were evaluated at an average temperature based on the highest and lowest thermocouple readings for a given distribution. This corresponded to the average temperature over the length δX. A sample calculation is contained in Appendix B.

The apparatus design is such that the height or radius of the tank could also be considered a characteristic dimension. The Grashof number thus becomes:

$$Gr_R = Gr_H = \frac{g\beta}{\nu^2} H^3 (T_s - T_b) \tag{7}$$

The test section radius was chosen to be one tenth the height of the tank. Or, in other words, the test section diameter was one fifth the height of the tank.

The various Grashof numbers are related according to:

$$Gr_R = 125Gr = Gr_H \tag{8}$$

3. Photographic Procedures

Many problems were encountered in photographing both the side view of the plume and the flow pattern on the circular section. The optical properties of both the plexiglass and the fluid interferred with focusing the camera. Existing lighting was not adequate. The red-orange color of the fluid masked the color change at the test surface. Several different cameras were used with a variety of lighting, filters and exposure settings.

The best results were obtained using a 35mm Honeywell Pentax camera with a Macro-Takumar lens (f/1.4 - 50mm focal length). Kodak Tri-X Pan film with ASA 400 was used. Pictures were developed using D-70 for 11 minutes at 68°F.

For photographs of the plume, the light from a 1000 watt Colortran Set Lamp (3200°K color temperature) was diffused through a white frosted ground glass plate that served as a background. Aperture setting of f/11 and f/16 at 1/30 second were used. Distance setting was 1.2 feet.

Pictures of the disk flow pattern were taken by centering the camera lens directly above the disk and resting the lens on the plexiglass tank top. An additional 300 watt Colortran Set Lamp (3200°K color temperature) was used to balance the light in the disk area. A distance setting of $9\frac{1}{2}$ inches was used. The aperture was set at f/4 and pictures taken at 1/15 and 1/30 second shutter speed.

IV. RESULTS AND DISCUSSION

A. REPRODUCIBILITY

It was found that a minimum of ten hours was necessary for any input setting to reach steady state. Once steady state was reached, very good agreement between Nusselt and Grashof Numbers based on test surface diameter obtained during the heating and cooling phase of the run resulted. Figure 5 is a Log-Log plot of the Nusselt number versus the Grashof number for a single data run. The uncertainty bands are shown on the plot.

For one run, the bulk temperature thermocouples were taped to the cylindrical container walls. This was done for two reasons; (1) to attempt to show the effect of wall temperature on the calculations and (2) to verify that the location of the bulk temperature thermocouples in the fluid did not appreciably effect the bulk temperature reading. Figure 6 is a Log-Log plot of Nusselt versus Grashof number showing data calculated based on this "wall" temperature, taken as the unit was cooling. For comparison, the cooling data results for the run conducted 19 Apr - 1 May 74 are shown. The agreement between the two data sets is excellent. Thus, the "wall" temperature measured was really an average bulk temperature and small changes in the bulk temperature thermocouple locations does not effect the results.

B. FLOW VISUALIZATION

The electrochemical flow visualization technique was successful at low input power settings. Figure 7 is a view of the flow pattern on the heated test surface at an input of 10.2 watts and a Grashof number based on test surface diameter of 1.4×10^6. Figure 8 shows the test surface

Figure 5. Data Comparison-Heating and Cooling Phase

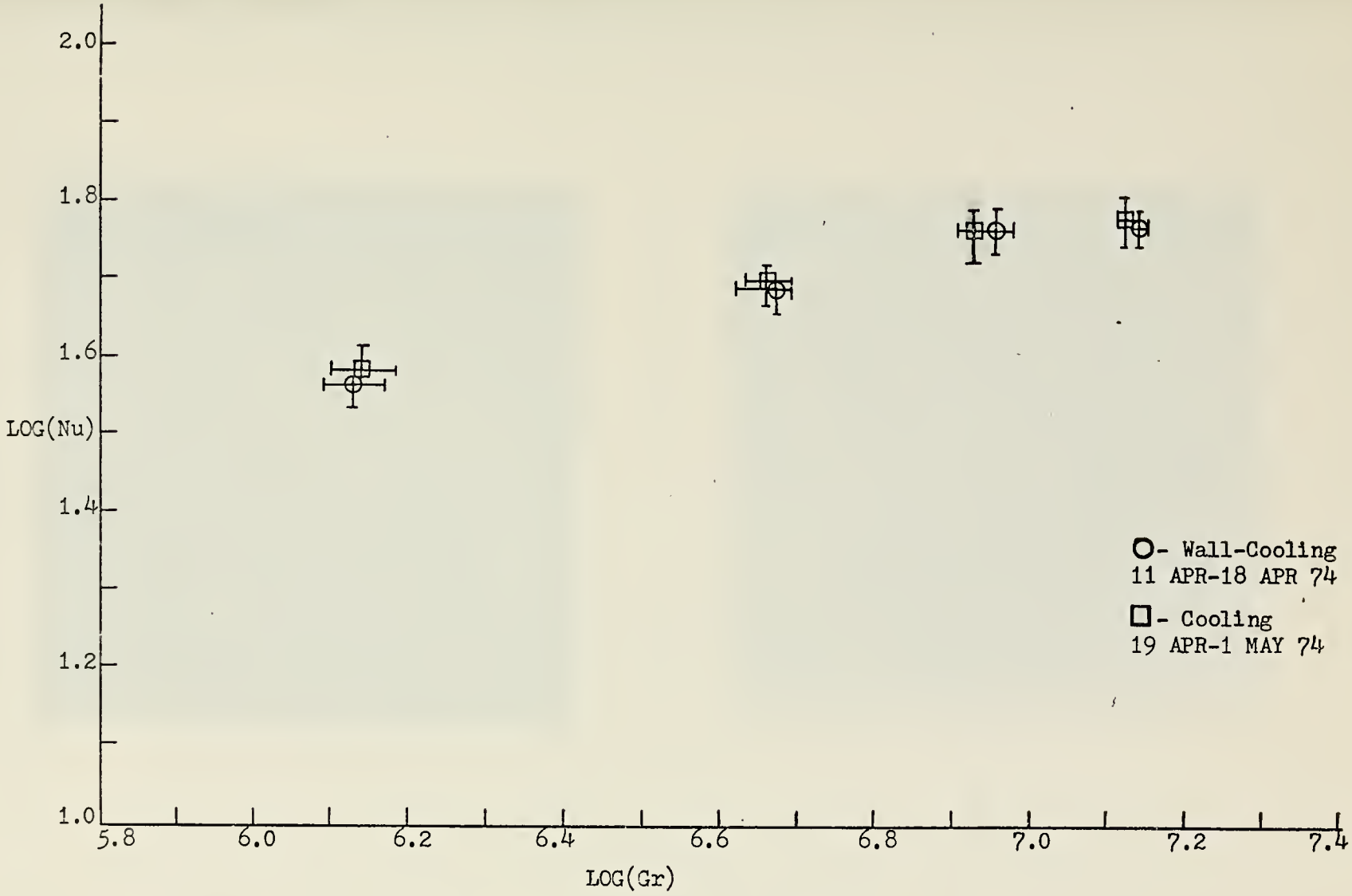

Figure 6. Data Comparison-Bulk Temperature Thermocouple Position

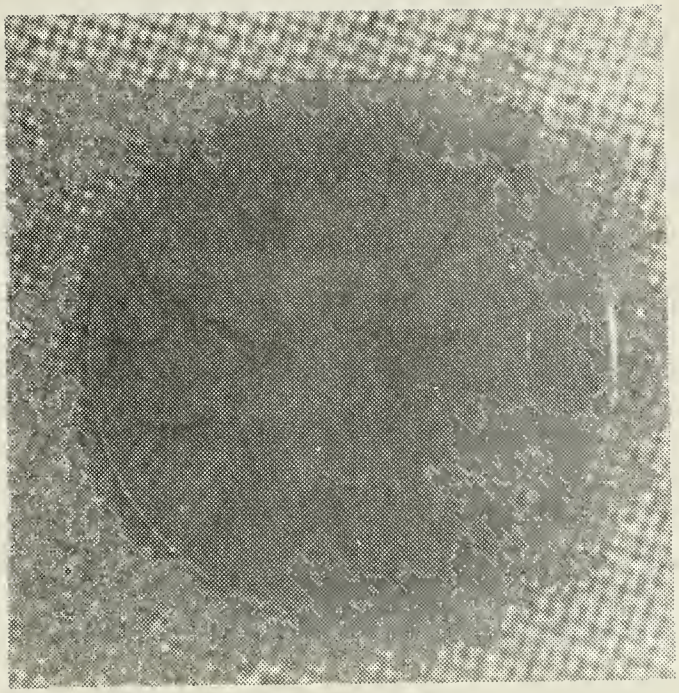

Figure 7. Test Surface; Gr = 1.4×10^6

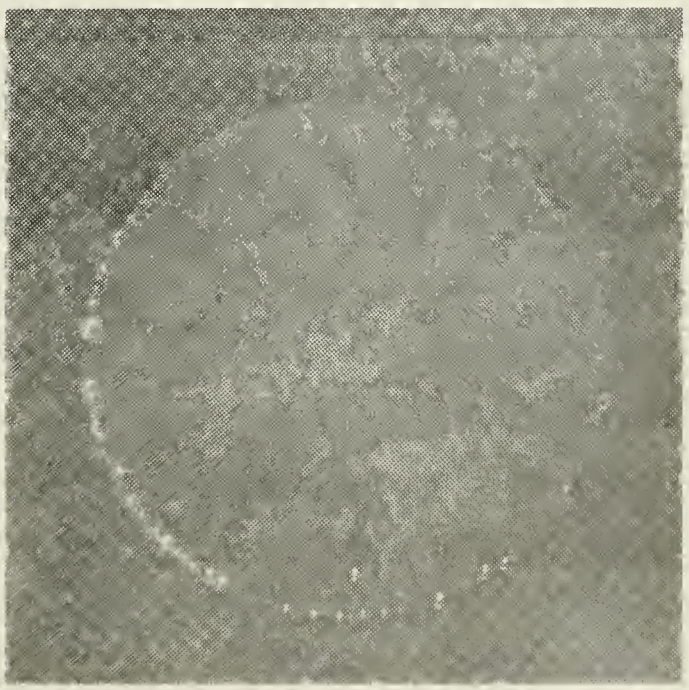

Figure 8. Test Surface; Gr = 4.6×10^6

at an input of 20.3 watts and a Grashof number of 4.6×10^6. In both of these photographs a symmetric cellular flow pattern is clearly evident. And as reported by Husar and Sparrow [12], the flow paths are convergent toward the center of the test section. It was observed that the number of cells in the cellular pattern increases with increasing Grashof number and this can be seen by examining the two photographs. It is noted that for the 20.3 watt setting bubbles were generated during the heating, but were confined to the circumference of the test section. These bubbles seem to have some minor effect on the flow pattern.

Figure 9 and Figure 10 are side views showing the plume at a Grashof number of 1.4×10^6. The flow is perpendicular to the test surface as it rises and laminar at this Grashof number. It was for the low input settings of 10.2 watts and 20.3 watts that the flow visualization could be accomplished using between 5 and 8 volts across the electrodes. At higher input settings, this voltage was not sufficient to produce the color change necessary for photographs. The flow could be seen and several observations could be made. It was established that the entire flow pattern was laminar at the 32.2 watt setting and turbulence was observed in the plume for both the 39.5 watt and the 45.1 watt settings. The Grashof numbers based on test surface diameter for these settings are 8.5×10^6, 1.3×10^7, and 1.8×10^7 respectively. This implies that the onset of turbulence occurs between the Grashof numbers based on test chamber height of 1.0×10^9 and 1.6×10^9. This is in agreement with Torrance's [21] observation of turbulence occurring at a Grashof number of 1.2×10^9.

The voltage across the electrodes was increased to improve the color change and disturbances in the flow pattern resulted. At first, very

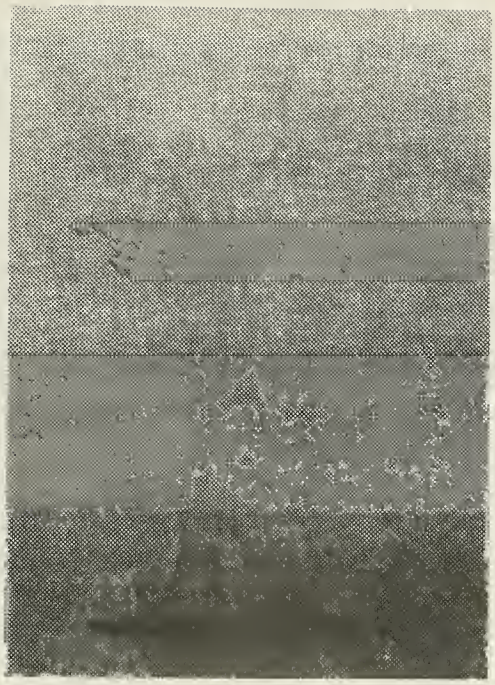

Figure 9. Plume; Gr = 1.4×10^6

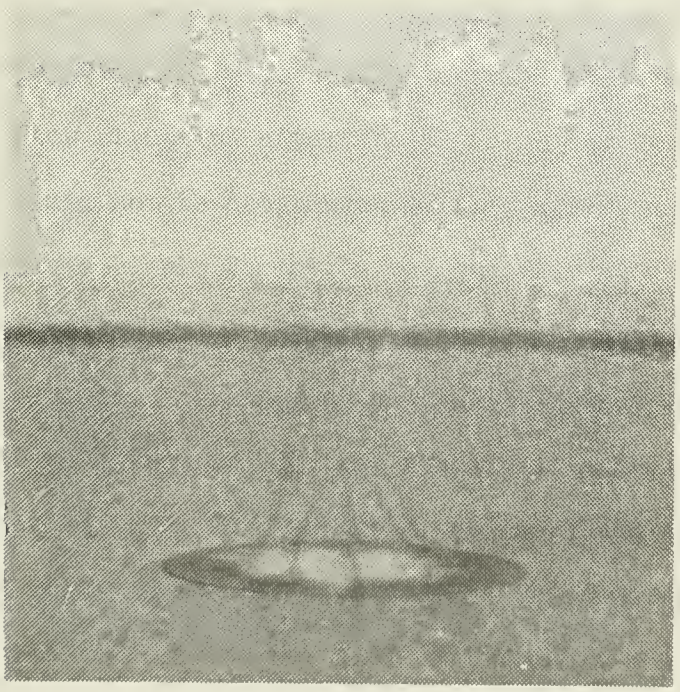

Figure 10. Plume; Gr = 1.4×10^6

small bubbles were observed that would break loose from the surface and disturb the flow. In trying to establish the voltage level necessary to cause this bubble formation another phenomena was observed. An increase in voltage apparently generated a sudden upward surge. Therefore, there were at least three different mechanisms that disturbed the flow: (1) bubbles due to heating, (2) bubbles due to electrode voltage and (3) an unexplained unsteadiness when electrode voltage was suddenly increased.

In considering these mechanisms the following statements based on experimental observation can be made. The three mechanisms are independent. They occur separately or together. Although bubbles do result from heating as shown in Figure 8, their effect on the flow pattern is minimal. It was found that this type of bubble formation is greatly diminished during the cooling phase of runs. Thus degassing the fluid should eliminate this problem.

It was stated previously that the flow was uneffected by a voltage of under 8 volts. Figure 11 is an example of the same flow situation as in Figure 9 but with 20 volts applied across the electrodes. Figure 12 is the same flow situation after the 20 volts has been applied for one minute. It could not be determined if this upward surge propagates or is cyclic because bubble formation begins after about one minute and further disturbs the flow. Figure 13 shows the presence of these bubbles on the test surface. Here again the flow situation is unchanged.

Figure 14 is a view of the test surface at a 39.5 watt input. The Grashof number is 1.3×10^7 and the plume turbulent when observed with only about 7 volts across the electrodes. This photograph was taken with 20 volts across the electrodes. All of the above mentioned mechanisms are influencing the flow pattern but the cellular pattern persists.

Figure 11. Plume; Gr = 1.4×10^6 (20 volts)

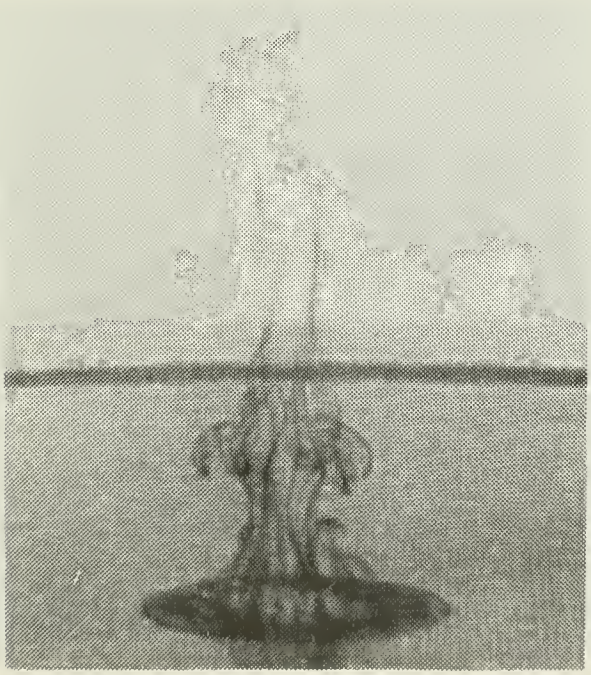

Figure 12. Plume; Gr = 1.4×10^6 (20 volts)

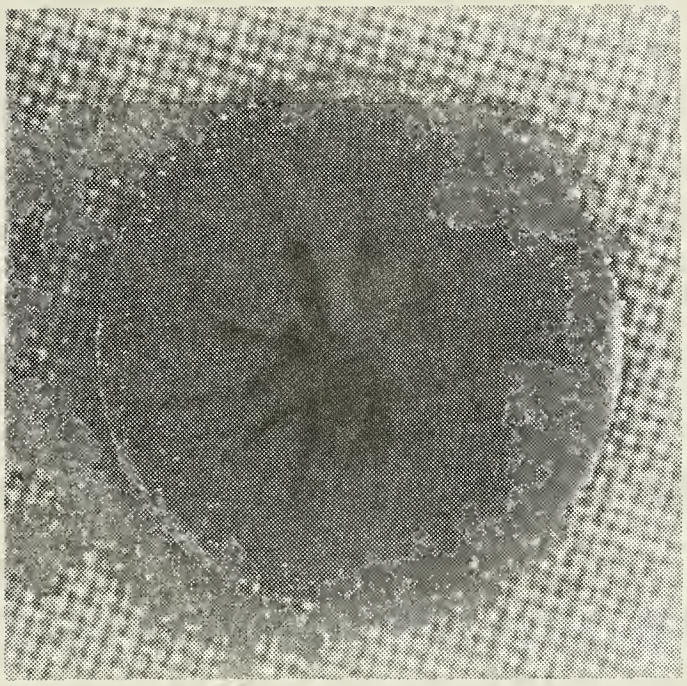

Figure 13. Test Surface; Gr = 1.4×10^6 (20 volts)

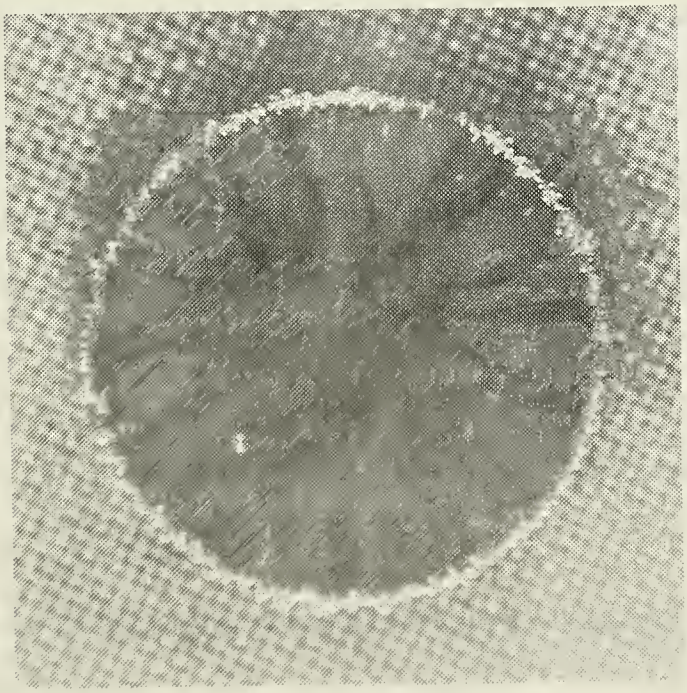

Figure 14. Test Surface; Gr = 1.3×10^7 (20 volts)

C. HEAT TRANSFER

The heat transfer results for each input setting are summarized for the various data runs in Table I. For each setting, the Nusselt, Grashof, and Rayleigh numbers were calculated. These dimensionless parameters were determined using the test surface diameter as the characteristic length. As described in the experimental procedure, data was taken at each setting as the apparatus was heated with increasing input and then again as inputs were decreased, cooling the test surface. Data taken during the cooling phase is denoted in the table. There is a trend in the data that shows the calculated Grashof numbers are higher for the cooling phase, but the Nusselt number seems unaffected. The data taken with the thermocouples taped to the cylindrical walls is also included in Table I. The data for this "wall run" is not significantly different from the other data. This was clearly seen in Figure 6 and the discussion on reproducibility.

A log-log plot of the Nusselt number versus the Rayleigh number based on test surface diameter for the data obtained experimentally is shown in Figure 15. The solid line is a least squares fit to the data. The Fortran computer subroutine, "LSQPL 2", from the U.S. Naval Postgraduate School computer center subroutine library was used to obtain this line. The heat transfer correlation which results from this experimental data is:

$$Nu = 0.97(Ra)^{0.24} \tag{9}$$

In Figure 15, the dashed line is the correlation reported by Duncan [24]

$$Nu = 0.31(Ra)^{0.30} \tag{10}$$

It is observed that the experimental data seems to agree reasonably well with Duncan's results for the two highest input power settings.

TABLE I

SUMMARY OF RESULTS

INPUT(WATT)	DATE	Nu	LOG(Nu)	Gr x 10^{-6}	LOG(Gr)	Ra x 10^{-6}	LOG(Ra)	TIME (hr)
10.2	21 MAR*	41.2	1.62	1.32	6.12	5.86	6.77	11.0
	2 APR	39.4	1.60	1.28	6.11	5.85	6.76	26.0
	5 APR(w)	39.5	1.60	1.18	6.07	5.54	6.74	14.0
	11 APR(w)	38.5	1.59	1.37	6.14	6.18	6.79	24.0
	18 APR*(w)	37.3	1.57	1.35	6.13	6.16	6.79	20.0
	19 APR	38.5	1.59	1.27	6.10	5.98	6.78	20.0
	29 APR*	38.8	1.59	1.39	6.14	6.12	6.78	17.0
20.3	21 MAR*	51.5	1.71	3.60	6.56	13.14	7.12	17.0
	6 APR(w)	50.7	1.71	3.36	6.53	12.42	7.09	20.0
	13 APR(w)	50.5	1.70	4.58	6.66	15.79	7.20	29.0
	17 APR*(w)	48.6	1.69	4.65	6.67	16.14	7.21	17.0
	22 APR	49.6	1.70	3.68	6.57	13.24	7.12	69.0
	28 APR*	49.7	1.70	4.60	6.66	16.00	7.20	25.0
32.2	8 APR(w)	56.9	1.76	8.15	6.91	24.46	7.39	24.0
	14 APR(w)	56.8	1.75	8.83	6.95	25.76	7.41	22.0
	16 APR*(w)	58.4	1.77	9.04	6.96	25.61	7.41	11.0
	25 APR	54.0	1.73	8.65	6.94	25.55	7.41	42.0
	27 APR*	58.5	1.77	8.50	6.93	24.66	7.39	26.0

* indicates cooling phase

(w) indicates "wall" run

TABLE I (continued)

SUMMARY OF RESULTS

INPUT(WATT)	DATE	Nu	LOG(Nu)	Gr x 10^{-6}	LOG(Gr)	Ra x 10^{-6}	LOG(Ra)	TIME (hr)
39.5	20 MAR*	61.5	1.79	12.40	7.09	33.53	7.52	16.0
	10 APR(w)	61.5	1.79	11.42	7.06	31.40	7.50	24.0
	15 APR(w)	59.0	1.77	13.75	7.14	36.02	7.56	14.0
	16 APR*(w)	59.4	1.77	13.77	7.14	36.08	7.56	14.0
	26 APR	61.2	1.79	12.86	7.11	34.33	7.54	22.0
	1 MAY*	60.3	1.78	13.10	7.12	34.97	7.54	22.0
45.1	15 APR(w)	63.6	1.80	17.69	7.25	43.34	7.64	11.0
	30 APR	62.1	1.79	18.12	7.26	44.39	7.65	18.5

* indicates cooling phase

(w) indicates "wall" run

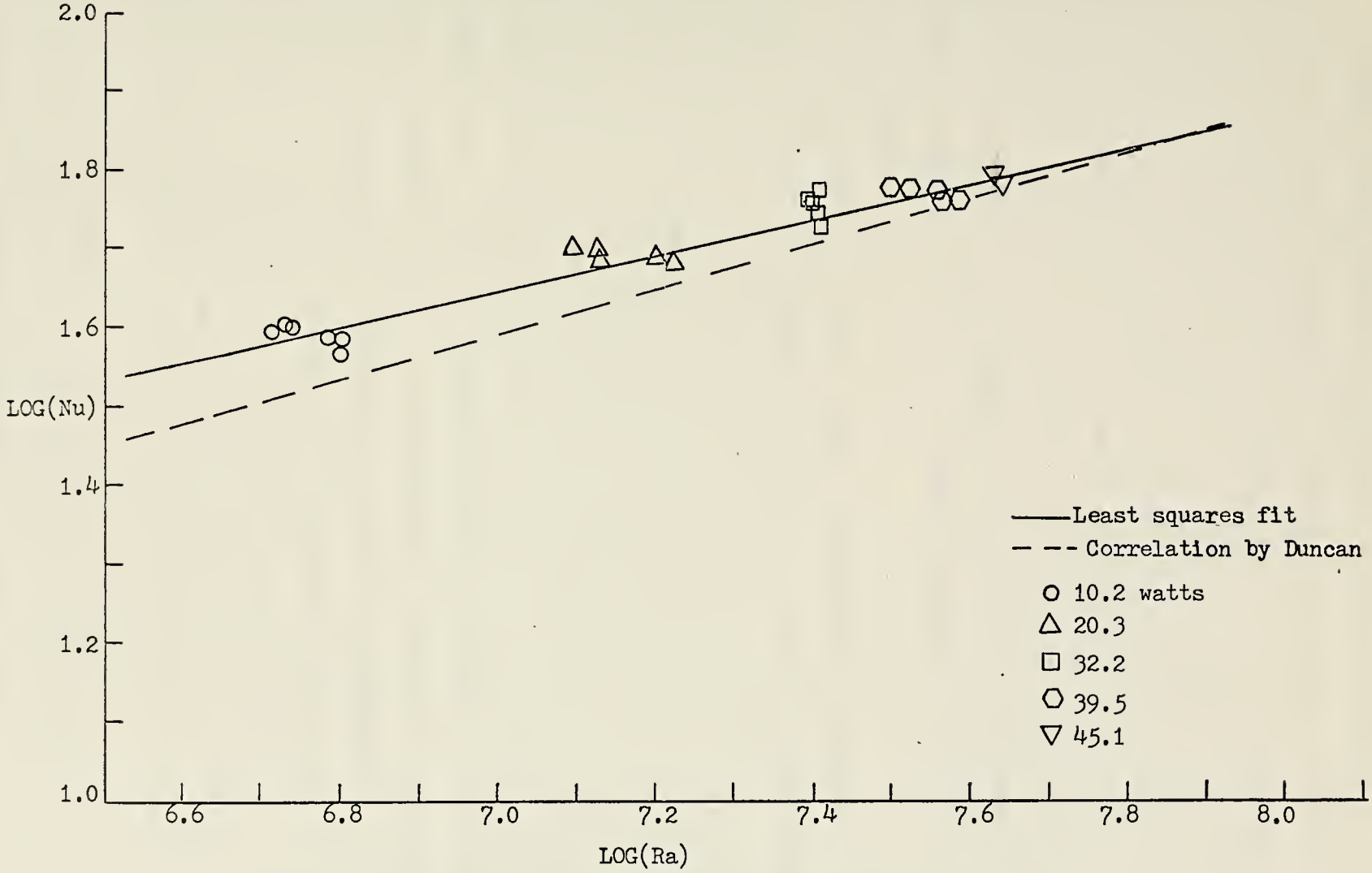

Figure 15. Correlation of Results Based on Rayleigh Number

Previous investigators have generally reported correlations with an exponent of 0.25 for laminar flow situations and 0.33 for turbulent flow. Since the flow visualization established that the two highest input settings were turbulent flow patterns, the data for these points should agree with the results of Duncan. Also Duncan's results include only two data points which can be considered in a laminar flow situation ($Ra < 8.5 \times 10^6$). Although not reported as such, his work seems for the most part to be in a turbulent range and his correlation reflects this. The results presented in this study indicate the greater portion of the data is in a laminar flow.

A log-log plot of Nusselt number versus Grashof number based on test surface diameter is presented in Figure 16. A least squares fit is also obtained for this data using "LSQPL2." The dashed line represents the theoretical results of Torrance [22]. The seemingly diverse results at the lower input settings should be looked at very closely. It should be noted that Torrance obtained good agreement between his numerical results [22] and his experimental data [21]. In his numerical solution, Torrance used a fluid bulk temperature that was assumed to be uniform. In his experimental work, this temperature was obtained as an average of the container wall temperature and the floor temperature. In this thesis work the bulk temperature was determined automatically as an average of the input of five thermocouples located in the fluid. It was felt that this method was not strongly influenced by any particular local temperature gradient. Whereas, Torrance's method could be dependent on the temperature gradients that occur in the floor section which surrounds the heated test surface. Considering this point in relation to the equations used to calculate the Nusselt and Grashof numbers, it is seen that

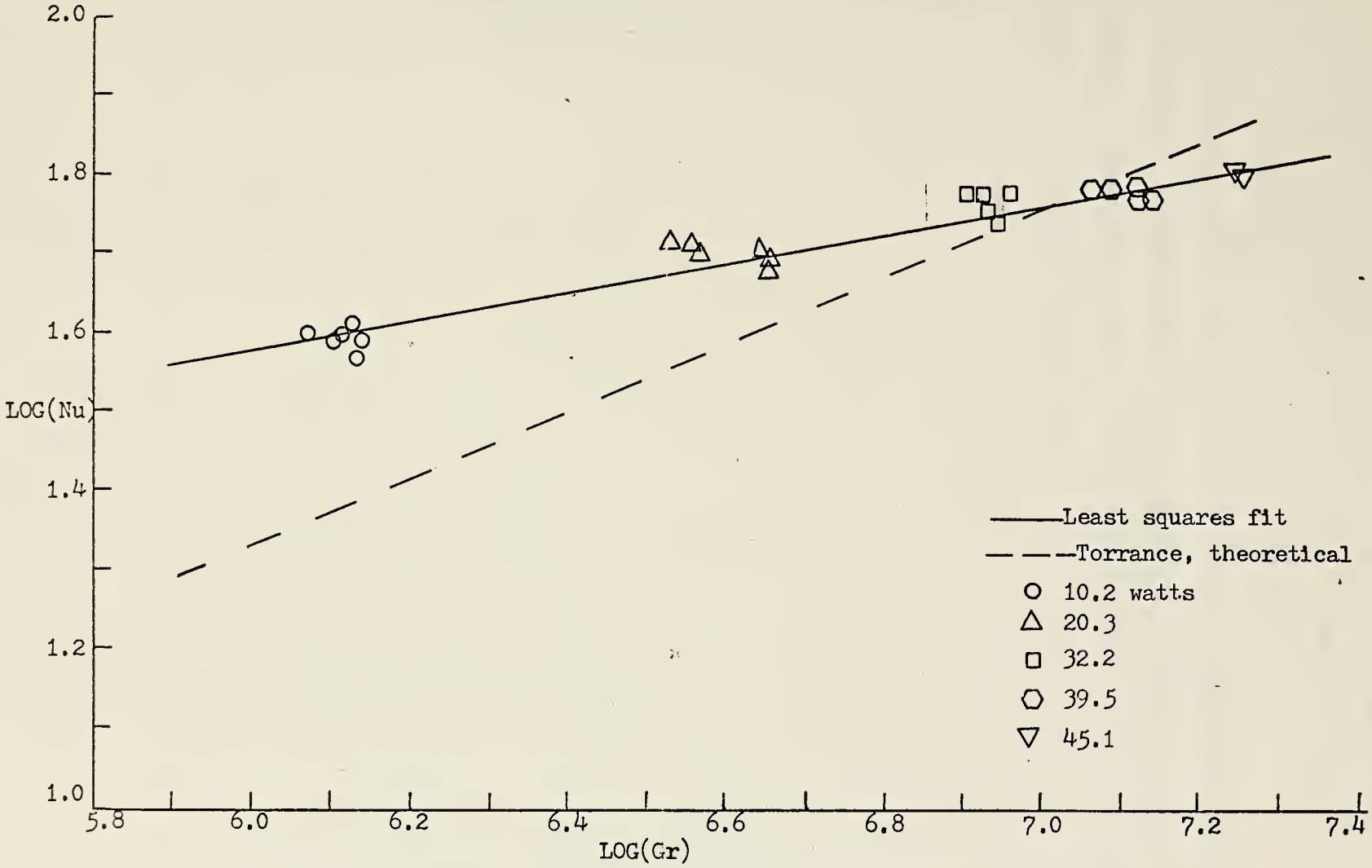

Figure 16. Correlation of Results Based on Grashof Number

a measurement resulting in a higher bulk temperature would shift the experimental data points closer to Torrance's result. The effect would not be as significant at the high input settings.

Torrance [22] also states that his numerical calculation was laminar and stable at a Grashof number based on chamber height of 4×10^9. When applied to this thesis study, the flow visualization shows that clearly the flow is unstable at this value.

V. CONCLUSIONS

1. The electrochemical flow visualization procedure can be used successfully at Grashof numbers less than 2.0×10^6. The voltage across the electrodes must be kept below 8 volts.

2. Disturbances can be introduced into the free convection flow by the voltage applied across the electrodes. These disturbances appear to originate from two independent mechanisms, (1) bubble formation and (2) sudden upward surge.

3. The transition of the plume from laminar to turbulent flow occurs in the Grashof number range from 8.5×10^6 to 1.3×10^7. It should be noted that the test surface diameter was used in the calculation of the Grashof numbers.

4. For a horizontal circular heated disk in a cylindrical enclosure, the following correlation is representative of heat transfer data in the Grashof number range of 1.2×10^6 to 1.8×10^7:

$$Nu = 0.97 \, (Ra)^{0.24} \tag{11}$$

5. An accurate determination of the temperature profile of the floor section surrounding the heated test surface is necessary to determine its effect on the fluid bulk temperature. If large temperature gradients occur, the measurement of bulk temperature profile would enable the heat loss, if any, to the floor to be calculated.

VI. RECOMMENDATIONS

A. DESIGN CHANGES

Input power to the heater had to be kept to under 50 watts. It was found that above this setting, very high temperatures occurred at the section of the apparatus where the stainless steel pipe support was bolted to the phenolic base plate. This problem results from heat being conducted through the stainless steel pipe section. A remedy to this problem would be to perforate the pipe section by drilling approximately 0.375 inch holes throughout its length while maintaining its rigidity.

Another problem encountered was the burnout of the heater lead connections inside the stainless steel pipe section. This can be avoided by by welding the junctions and insulating the leads from the stainless steel pipe section.

During the experimental runs, thermal expansion of the heater - test section occurred at high power input settings. Using the three threaded support rods to bring the phenolic bottom level with the test surface was time consuming. Because of the "O" ring sealing around the test section, the phenolic plate did not slide freely. This problem could have been corrected by installing a nut and bolt level adjustment at the base of the pipe section at the stainless steel ring.

The phenolic plate that served as the tank bottom discolored and seemed to be losing its finish. Also it happens to be very nearly the same color as the test fluid, this led to problems with photographic contrast. Using a material such as bakelite or painting this surface with a heat resistant paint may be possible alternatives which can be considered. Also using six threaded rods to provide a watertight seal

interferred to some extent with the option of photographing from different positions. Using fewer rods or grouping existing rods closer together with a larger space between groups would alleviate the problem.

B. FUTURE WORK

The flow visualization technique can be applied to surfaces with artificial cavities and the result compared to the results of this study.

A drawback of the use of thymol blue sodium salt for this flow visualization technique is the deep orange-yellow color of the fluid. Preliminary work using phenolphthalein, which is colorless in acid and red when basic, shows a similar flow visualization can be obtained. Problems such as undissolved solid and optimum percent weight to use must be resolved.

Recent advances in the measurement of temperature using liquid crystals can be applied to this apparatus. Methods of liquid crystal application to the test surface must be devised. The data obtained in this study can be used to determine the temperature range of the liquid crystals for a given input point. The liquid crystals can also be used to determine the temperature profile of the floor surrounding the heated test surface.

A study should be undertaken to determine as near as possible the Grashof number at which the onset of turbulence occurs. Correlations can then be developed based on a laminar or turbulent flow behavior.

The affect of voltage on free convection flow can be studied in greater detail, and an effort made to isolate the mechanisms that come into play. This will be necessary if the electrochemical flow visualization is to be used in a similar apparatus design at high Grashof numbers.

Appendix A. Thermocouple Calibration Procedure

The accurate determination of the fluid and test section temperatures was an absolute necessity in this experiment. For this reason, calibration of the sheathed and bulk temperature thermocouples was required. The calibration was accomplished with all instrumentation components that would be used when the apparatus was operating. In other words, there were no wiring or recording instrument changes once the system was calibrated.

A Rosemount Calibration System, with a constant temperature oil bath, was used for the calibration. The ice junction thermocouple which was sealed in a glass tube filled with oil was placed in a stainless steel dewar with a constant circulation pump. The five bulk temperature thermocouples and the four sheathed thermocouples were suspended several inches into the oil bath. A Platinum Resistance Thermometer in conjunction with a commutation bridge was used as a standard. The calibration was conducted over a range from $40^{\circ}F$ to $215^{\circ}F$. The maximum error for the thermometer for this temperature range was $0.004^{\circ}C$.

The results of the calibration were compared with standard thermocouple tables. There was good agreement between the table values and the calibration results for the sheathed thermocouples. The deviation from the table values ranged from -0.010 mv to +0.011 mv. The bulk temperature results were consistently higher than the table values. The deviation ranged from +0.001 mv to +0.020 mv.

The decision was made to utilize the standard tables and assume an uncertainty in the sheathed thermocouple reading of $0.5^{\circ}F$ and an uncertainty of $1.0^{\circ}F$ in the bulk temperature reading.

Appendix B. Sample Calculations

Input 20.3 watts (data recorded 21 March 1974):

A. Determination of the surface temperature

A graphical method was used to determine the surface temperature. For each input setting a plot of the temperature versus the thermocouple distance from the surface, as shown in Figure 17, was made. The plots were linear and the surface temperature could be obtained to within $0.5^{o}F$.

B. Calculation of the Nusselt number

Using the equations:

$$h = \frac{K(T_{11}-T_8)}{\delta X(T_s-T_b)} \tag{12}$$

and

$$Nu = \frac{hD}{K_f} \tag{13}$$

the Nusselt number was determined. The value of K was determined for an average temperature of the cylinder over the length δX. The average of the highest and lowest temperature in the cylinder was used. The value of K was obtained from a plot of temperature versus K based on values from Touloukian [26]. Fluid properties were evaluated at the film temperature (equation 6) in a similar manner from properties listed in Holman's text [27]. The following were obtained for the 20.3 watts input settings:

$K = 9.65$ BTU/hr/ft/^{o}F

$g\beta/\nu^2 = 2.1 \times 10^8$ 1/ft^3/^{o}F

$Pr = 3.65$

$K_f = 0.3715$ BTU/hr/ft/^{o}F

$\delta X = 0.125$ ft

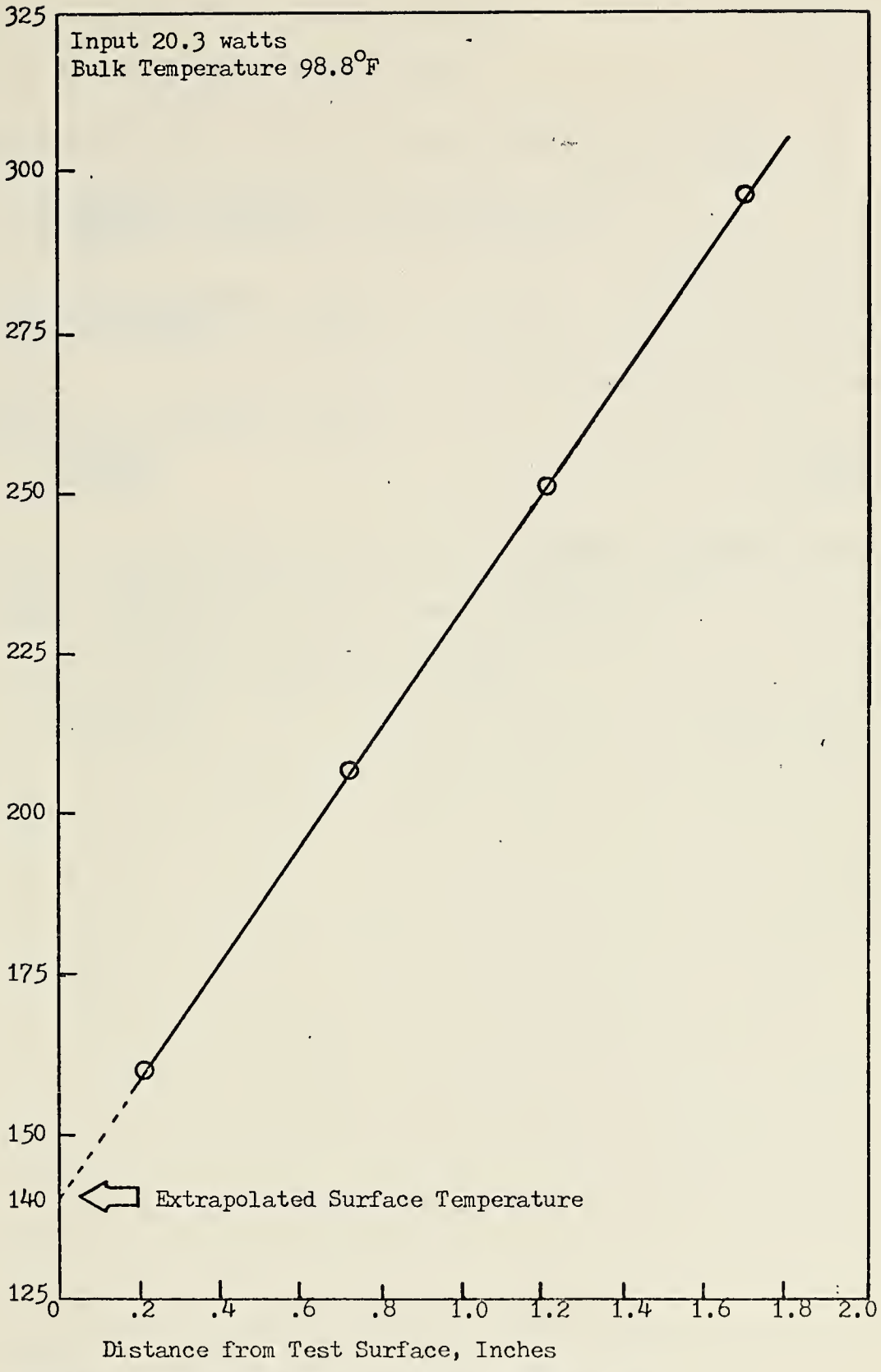

Figure 17. Determination of Surface Temperature

$$\delta T_c = T_{11} - T_8 = 297.5 - 160.8 = 136.7^{\circ}F$$

$$\delta T = T_s - T_b = 140.0 - 98.8 = 41.2^{\circ}F$$

Using equations (12) and (13), the Nusselt number is obtained:

$$h = \frac{9.65(297.5 - 160.8)}{0.125(140.0 - 98.8)} = 256.15 \text{ BTU/hr/ft}^2/^{\circ}F$$

$$Nu = \frac{256.15(0.07466)}{0.3715} = 51.48$$

C. Calculation of the Grashof number

$$Gr = \frac{g\beta D^3 \delta T}{\nu^2} \qquad (14)$$

Values for $\frac{g\beta}{\nu^2}$ were determined from Holman's text [27]. For the 20.3 watt input setting, using equation (14) the Grashof number is:

$$Gr = 2.1 \times 10^8 \ (0.000416)(140.0 - 98.8)$$

$$Gr = 3.6 \times 10^6$$

Appendix C. Uncertainty Analysis

Uncertainties in this experimental work were treated by the method proposed by Kline and McClintock [28].

Several assumptions and approximations had to be made in order to develop a reasonable estimate of the uncertainties for each variable. Table II is a summary of these uncertainties.

TABLE II

UNCERTAINTY OF VARIABLES

VARIABLE	UNCERTAINTY (W) (odds 20 to 1)	BASIS FOR VALUE
δX	0.00042 ft	accuracy of measurement
$g\beta/\nu^2$	$0.10 \times 10^8/ft^3/^oF$	assumption based on table values [27]
$K_f(H_2O)$	0.001 BTU/hr/ft/^oF	assumption based on table values [27]
K(304 stainless)	5 percent	[26]
T_s	0.5^oF	dictated by scale of graphical method
T_b	1.0^oF	thermocouple calibration
T_8, T_{11}	0.5^oF	thermocouple calibration
D	0.0002 inch	accuracy of measurement

The second-power equation of Kline and McClintock [28] was used for the calculation of uncertainties in the values obtained experimentally.

The uncertainties in the temperature differences δT_c and δT were calculated from

$$W_{\delta T} = \left[(W_{T_s})^2 + (W_{T_b})^2\right]^{\frac{1}{2}} = \left[(0.5)^2 + (1.0)^2\right]^{\frac{1}{2}} = 1.12^oF \text{ (odds 20 to 1)} \quad (15)$$

$$W_{\delta T_c} = \left[(W_{T_8})^2 + (W_{T_{11}})^2\right]^{\frac{1}{2}} = \left[(0.5)^2 + (0.5)^2\right]^{\frac{1}{2}} = 0.707^oF \text{ (odds 20 to 1)} \quad (16)$$

Where W_{T_s} = uncertainty in T_s

W_{T_b} = uncertainty in T_b

Uncertainty in the convective heat transfer coefficient (h) was determined using

$$\frac{W_h}{h} = \left[\left(\frac{W_K}{K}\right)^2 + \left(\frac{W_{\delta T_c}}{\delta T_c}\right)^2 + \left(\frac{W_{\delta X}}{\delta X}\right)^2 + \left(\frac{W_{\delta T}}{\delta T}\right)^2\right]^{\frac{1}{2}} \tag{17}$$

The uncertainties (W) are obtained from Table II.

Since the Nusselt number is defined:

$$Nu = \frac{hD}{K_f} \tag{18}$$

the second power equation for uncertainty in this number becomes

$$\frac{W_{Nu}}{Nu} = \left[\left(\frac{W_h}{h}\right)^2 + \left(\frac{W_D}{D}\right)^2 + \left(\frac{W_{K_f}}{K_f}\right)^2\right]^{\frac{1}{2}} \tag{19}$$

It can be shown that the terms $\left(\frac{W_D}{D}\right)^2$ and $\left(\frac{W_{K_f}}{K_f}\right)^2$ are very small and can be neglected. Therefore,

$$\frac{W_{Nu}}{Nu} = \frac{W_h}{h} \tag{20}$$

In determining the uncertainty in the calculation of the Grashof number, the equation reduces to

$$\frac{W_{Gr}}{Gr} = \left[\left(\frac{Wg\beta/\nu^2}{g\beta/\nu^2}\right)^2 + \left(\frac{3W_D}{D}\right)^2 + \left(\frac{W_{\delta T}}{\delta T}\right)^2\right]^{\frac{1}{2}} \tag{21}$$

Table III summarizes the results of this analysis for a representative run.

TABLE III

UNCERTAINTIES IN THE EXPERIMENT

Input Setting (Watts)	Percent Uncertainty	
	Nusselt Number	Grashof Number
10.2	7%	10%
20.3	6%	6%
32.2	6%	4%
39.5	5%	3%
45.1	5%	3%

BIBLIOGRAPHY

1. Ostrach, S., "Natural Convection in Enclosures," Advances in Heat Transfer, v. 8, p. 161-227, 1972.

2. Edwards, D. K. and Catton, I., "Prediction of Heat Transfer by Natural Convection in Closed Cylinders Heated From Below," Int. J. Heat Mass Transfer, v. 12, p. 23-30, January 1969.

3. Catton, I. and Edwards, D. K., "Initiation of Thermal Convection in Finite Right Circular Cylinders," A I Ch E, v. 16, no. 4, p. 594-601, July 1970.

4. Charlson, G. S. and Sani, R. L., "Thermoconvective Instability in a Bounded Cylindrical Fluid Layer," Int. J. Heat Mass Transfer, v. 13, p. 1479-1496, September 1970.

5. Lawrence Livermore Laboratory, University of California, Livermore UCRL - 51146, Numerical Studies of Laminar, Free Convection in a Horizontal Fluid Layer Heated From Below, by W. H. Plows, 5 January 1972.

6. Stork, J. and Muller, U., "Convection in Boxes: Experiments," Journal of Fluid Mechanics, v. 54, part 4, p. 599-611, 1972.

7. Szekely, J. and Todd, M. R., "Natural Convection in a Rectangular Cavity Transient Behavior and Two Phase Systems in Laminar Flow," Int. J. Heat Mass Transfer, v. 14, p. 467-482, March 1971.

8. Gebhart, B., Pera, L. and Schorr, A. W., "Steady Laminar Natural Convection Plumes Above a Horizontal Line Heat Source," Int. J. Heat Mass Transfer, v. 13, p. 161-171, 1970.

9. Pera, L. and Gebhart, B., "On the Stability of Laminar Plumes; Some Numerical Solutions and Experiments," Int. J. Heat Mass Transfer, v. 14, p. 975-984, July 1971.

10. Fujii, T., Morioku, I. and Uehara, H., "Buoyant Plume Above a Horizontal Line Heat Source," Int. J. Heat Mass Transfer, v. 16, p. 755-768, April 1973.

11. Lloyd, J. R., Sparrow, E. M. and Eckert, E. R. C., "Laminar, Transition and Turbulent Natural Convection Adjacent to Inclined Vertical Plates," Int. J. Heat Mass Transfer, v. 15, p. 457-475, March 1972.

12. Husar, R. B. and Sparrow, E. M., "Patterns of Free Convection Flow Adjacent to Horizontal Heated Surfaces," Int. J. Heat Mass Transfer, v. 11, p. 1206-1208, July 1968.

13. Baker, J. D., "A Precise Measurement of Small Fluid Velocities," Journal of Fluid Mechanics, v. 26, part 3, p. 573-575, 1966.

14. Hahne, E. W. P., "Heat Transfer and Natural Convection Patterns on a Horizontal Circular Plate," Int. J. Heat Mass Transfer, v. 12, p. 651-652, May 1969.

15. Wragg, A. A. and Looma, R. P., "Free Convection Flow Patterns at Horizontal Surfaces with Ionic Mass Transfer," Int. J. Heat Mass Transfer, v. 13, p. 439-442, February 1970.

16. Goldstein, R. J., Sparrow, E. M. and Jones, D. C. "Natural Convection Mass Transfer Adjacent to Horizontal Plates," Int. J. Heat Mass Transfer, v. 16, p. 1025-1035, May 1973.

17. Fishenden, M. and Saunders, O. A., An Introduction to Heat Transfer, Oxford, 1950.

18. Mikheyev, M., Fundamentals of Heat Transfer, p. 77-78, Peace Publishers, Moscow, 1968.

19. Hassan, K. and Mohamed, S., "Natural Convection from Isothermal Flat Surfaces," Int. J. Heat Mass Transfer, v. 13, p. 1873-1886, December 1970.

20. Sparrow, E. M., Husar, R. B. and Goldstein, R. J., "Observations and other Characteristics of Thermals," Journal of Fluid Mechanics, v. 41, part 4, p. 793-800, 1970.

21. Torrance, K. E., Orloff, L. and Rockett, J. A., "Experiments on Natural Convection in Enclosures with Localized Heating from Below," Journal of Fluid Mechanics, v. 36, part 1, p. 21-31, 1969.

22. Torrance, K. E., Orloff, L. and Rockett, J. A., "Numerical Study of Natural Convection in an Enclosure with Localized Heating from Below --- Creeping Flow to the Onset of Laminar Instability," Journal of Fluid Mechanics, v. 36, part 1, p. 33-54, 1969.

23. Lee, S. L. and Hellman, J. M., Advances in Heat Transfer, v. 10, p. 220-281, 1974.

24. Duncan, D. S., Natural Convection Heat Transfer From a Horizontal Disk in a Cylindrical Enclosure, M. S. Thesis, Naval Postgraduate School, Monterey, California, 1971.

25. MacKenzie, D. K., Vaporization of Thin Liquid Films, M. S. Thesis, Naval Postgraduate School, Monterey, California, 1972.

26. Touloukian, Y. S., and others, Thermophysical Properties of Matter, v. 16, I F I/Plenum, 1970.

27. Holman, J. P., Heat Transfer, 3rd ed., McGraw-Hill, 1972.

28. Kline, S. J. and McClintock, F. A., Describing Uncertainties in Single Sample Experiments," Mechanical Engineering, v. 75, p. 3-8, January 1953.

INITIAL DISTRIBUTION LIST

		No. Copies
1.	Defense Documentation Center Cameron Station Alexandria, Virginia 22314	2
2.	Library, Code 0212 Naval Postgraduate School Monterey, California 93940	2
3.	Assoc. Professor M. D. Kelleher Department of Mechanical Engineering Naval Postgraduate School Monterey, California 93940	1
4.	Department of Mechanical Engineering Code 59 Naval Postgraduate School Monterey, California 93940	1
5.	LT Joseph M. O'Connor 2 General Street Providence, Rhode Island 02904	1